Evaluation of Narrowband and Broadband Vegetation Indices for Determining Optimal Hyperspectral Wavebands for Agricultural Crop Characterization

Prasad S. Thenkabail, Ronald B. Smith, and Eddy De Pauw

Abstract

The main goal of the study was to determine optimal waveband centers and widths required to best estimate agricultural crop characteristics. The hyperspectral narrowband data was acquired over 395 to 1010 nanometers using a 1.43-nanometer-wide, 430 bands, hand-held spectroradiometer. Broadband data were derived using a Landsat-5 Thematic Mapper image acquired to correspond with field spectroradiometer and ground-truth measurements. Spectral and biophysical data were obtained from 196 sample locations, including farms and rangelands. Six representative crops grown during the main cropping season were selected: barley, wheat, lentil, cumin, chickpea, and vetch. Biophysical variables consisted of leaf area index, wet biomass, dry biomass, plant height, plant nitrogen, and canopy cover.

Narrowband and broadband vegetation indices were computed and their relationship with quantitative crop characteristics were established and compared. The simple narrowband two-band vegetation indices (TBVI) and the optimum multiple-band vegetation indices (OMBVI) models provided the best results. The narrowband TBVI and OMBVI models are compared with six other categories of narrow and broadband indices. Compared to the best broadband TM indices, TBVI explained up to 24 percent greater variability and OMBVI explained up to 27 percent greater variability in estimating different crop variables. A Predominant proportion of crop characteristics are best estimated using data from four narrowbands, in order of importance, centered around 675 nanometers (red absorption maxima), 905 nm (near-infrared reflection peak), 720 nm (mid portion of the red-edge), and 550 nm (green reflectance maxima). The study determined 12 spectral bands and their bandwidths (Table 5) that provide optimal agricultural crop characteristics in the visible and near-infrared portion of the spectrum.

Introduction, Background, and Rationale

Until recently, Earth Observation Satellites carried only broadwaveband sensors such as the Landsat Enhanced Thematic Mapper (ETM+), Thematic Mapper (TM), Multispectral Scanner (MSS), Le Systémé pour l'observation de la terre (SPOT) high resolution visible (HRV), and the Indian Remote Sensing (IRS) Linear Imaging Self-Scanning (LISS). These sensors have known limitations in providing adequate information on terrestrial ecosystem characteristics such as in providing accurate estimates of biophysical and yield characteristics of agricultural crops (e.g., Richardson *et al.*, 1992; Weigand *et al.*, 1992; Gong *et al.*, 1995; Thenkabail *et al.*, 1995; Carter, 1998; Lyon *et al.*, 1998; Shaw *et al.*, 1998; Asner *et al.*, 2000), and crop type or species identification (Asner *et al.*, 2000). Limitations such as these have led to an increasing interest in the narrow-waveband sensors, which are expected to provide information that is more detailed and/or enable a host of new applications. The recent successful launches of Terra, the Earth Observing System (EOS) flagship satellite, and the Earth Observing-1 (EO-1) usher a new era of hyperspectral observations of the Earth from space. EO-1 carries the Hyperion sensor with 220 narrowbands, each of 10-nm width. Upcoming hyperspectral sensor launches also include 105 narrow wavebands in the Australian Resource Information and Environment Satellite (ARIES), and the Warfighter-1 with 200 narrow wavebands in a sensor onboard the United States private industry satellite Orbview-4. All these sensors cover the 400- to 2500-nanometer spectral range. In the past, there has been significant experience in the use of near-continuous spectra from imaging spectrometers such as the NASA-designed Airborne Visible-Infrared Imaging Spectrometer (AVIRIS) and Compact Airborne Spectrographic Imager (CASI). The Hyperion and other hyperspectral sensors will produce very large data volumes, which make it imperative that newer methods and techniques be developed to handle these multi-dimensional datasets.

Even better will be to focus on the design of an optimal sensor for a given application by dropping redundant bands. Optimal hyperspectral sensors will help reduce data volumes, eliminate the problems of high-dimensionality of hyperspectral datasets, and make it feasible to apply traditional classification methods to a few selected bands (optimal bands) that capture most of the information regarding crop characteristics. Future generations of satellites are either likely to carry specialized optimal sensors focused on gathering data for targeted applications, or to carry a narrow-waveband hyperspectral sensor such as Hyperion from which users with different application needs can extract appropriate optimal wavebands. Thereby, knowledge of

P.S. Thenkabail and R.B. Smith are with the Center for Earth Observation (CEO), Yale University, P.O. Box 208109, New Haven, CT 06511 (prasad.thenkabail@yale.edu; ronald.smith@yale.edu).

E. De Pauw is with the International Center for Agricultural Research in the Dry Areas (ICARDA), Aleppo, Syria (e.de-pauw@cgiar.org).

application specific "optimal bands" for multi-dimensional datasets such as Hyperion and Warfighter-1 is mandatory in order to reduce costs in data analysis and computer resources. Table 1 compares the spectral and spatial resolution of narrowband and broadband data used in this study with the characteristics of well-known narrowband AVIRIS airborne and recently launched Hyperion space-borne sensors. A number of recent studies have indicated the advantages of using discrete narrowband data from specific portions of the spectrum when compared with broadband data in order to arrive at optimal quantitative or qualitative information regarding crop or vegetation characteristics (e.g., Elvidge and Chen, 1995; Carter, 1998; Blackburn, 1999; and Thenkabail et al., 2000b).

The Main goal of this paper was to determine the optimal hyperspectral narrow wavebands, in the visible and near-infrared portion of the spectrum, that best characterize agricultural crop characteristics. Vegetation indices derived from narrow and broad wavebands were used to establish relationships with crop biophysical variables and yield. Data were acquired from 176 farmer- or researcher-managed farms and 20 marginal land (or rangeland) plots in the arid and semi-arid environments of Syria using (1) narrow waveband data from 512 1.43-nanometer-wide discrete narrowbands in the visible and NIR portion (350 to 1050 nanometers) of the spectrum, and (2) broad waveband data from the six non-thermal bands (450 to 2350 nm) of the Landsat-5 TM sensor. The study was conducted during April and May, 1998 during the main (spring) cropping season.

Study Area

The study area is located around Aleppo, Syria in the desert margins of southwest Asia where agriculture faces complex challenges due to inadequate rainfall. The long-term mean rainfall during the effective growing season of November through May is 373 mm. Approximately 50 percent of the work force earns its living directly from agriculture, placing great stress on the sustainability of land and water resources. Worldwide, an estimated one billion people currently live in countries and regions included in the desert margins with population growth rates of 2.1 percent in the Central Asian Republics and 3.6 percent in the Mediterranean regions. The bounding coordinates of the study area are, in Syria: upper left: 36.30N, 36.50E; upper right: 36.30N, 37.43E; lower right: 35.56N, 37.43E; and lower left: 35.56N, 36.50E. The study area consists of researcher-managed and farmer-managed farms growing mainly cereals

(wheat, barley) and legumes (vetch, lentil, chickpea) intermingled with cumin, fallow farms, and rangelands in the main crop-growing season.

Methods and Procedures

Narrowband, broadband, and ground-truth data were extracted from 196 specific locations spread across the study area in farmer- and researcher-managed farms and marginal lands. Sample sites were located using a Garmin™ Global Positioning System (GPS) receiver and consisted of barley (44 sample locations), wheat (64), lentil (23), cumin (17), chickpea (14), vetch (14), marginal lands (20), and fallow farms or top soils (9).

Hyperspectral Data

Narrowband data were gathered to coincide with Landsat-5 TM broadband acquisition. Narrowband data were acquired from 13 April through 05 May 1998 using a hand-held spectroradiometer manufactured by Analytical Spectral Devices™, which provided data in 512 1.43-nm-wide discrete narrowbands in the visible and near-infrared (332- to 1064-nm) bands. A detailed description of the spectroradiometer instrument is given by FieldSpec (1997), Thenkabail et al. (1999), and Thenkabail et al. (2000). Reflectance using the spectroradiometer is calculated by

Reflectance

$$= ((\text{target-dark current})/(\text{reference-dark current}))*100 \text{ percent.}$$

Spectral data from the spectroradiometer and quantitative and qualitative data on crops and on soils were obtained from 196 ground-truth locations spread across the study area. Measurements were made at a nadir-looking 18-degree field of view (FOV) between 1000 and 1100 local time each day to keep the sun angle effects consistent. All measurements were taken under bright clear-sky conditions. All canopy-level measurements were acquired at a height of approximately 1.20 m above the ground with a 38-cm-diameter footprint on the ground, resulting in an area of 1134 cm² observed on ground. Each acquired spectra included an average of ten individual measurements that were automatically acquired by the FieldSpec spectroradiometer. Narrowband reflectivity obtained at ground level is mostly free of atmospheric effects. The mean hyperspectral characteristics of six agricultural crops, rangelands,

TABLE 1. CHARACTERISTICS OF THE SENSORS. NARROWBAND AND BROADBAND DATA USED IN THIS STUDY COMPARED WITH SPACEBORNE HYPERION AND AIRBORNE AVIRIS SENSORS

Sensor	wavelength (nanometers)	spectral resolution (nanometers)	number of bands (#)	spatial resolution (meters)	area per pixel (m²)	pixels per hectare (#)
1. Narrow band data for this study from Spectroradiometer (visible and NIR)	395–1010*	1.43	430	0.38**	0.1133**	88219
2. Broad band data for this study from Landst-5 TM	450–2350	band 1: 70 nm band 2: 80 nm band 3: 60 nm band 4: 140 nm band 5: 20 nm band 7: 27 nm	6	30	900	11.11
3. Hyperion	400–2500	10	220	30	900	11.11
4. AVIRIS	400–2500	10	224	20	400	25

Note: *Visible and near infrared (VNIR) spectroradiometer is in the 350- to 1050-nm range. However, only the 395- to 1010-nm range of the spectrum was considered in order to avoid the significant noise in the early and late waveband portions.
**Area when the spectroradiometer was held at 1.2 meter above ground level with an 18 degree field of view (FOV), resulting in a diameter of 0.38 m and area (πr^2) of 0.113354 m² (or 1133 cm²).

and fallow farms are plotted in Figure 1. The representative growth stages of crops are varied from late vegetative to critical in most cases (Figure 1).

Broadband Data
Broadband data were extracted from an 06 April 1998 Landsat-5 TM image. Mean digital values for the six non-thermal bands were extracted from a 3- by 3-pixel area from each of the 196 sample site locations. The GPS location is centered on this 3- by 3-pixel area. Broadband data were also derived simulating the discrete narrowband data of the spectroradiometer (which are free from atmospheric effects because the data are acquired at ground level). Preliminary investigations showed that the simulated broadband data provided results significantly similar to atmospherically resistant at-satellite exo-atmospheric reflectance-based Landsat-5 TM broadband data in their relationships with agricultural crop variables. In addition, in a recent study Thenkabail *et al.* (1999; 2000b) performed a detailed comparison of the simulated broadband TM data with the narrowband data. Therefore, only the broadband data derived from the Landsat-5 TM sensor have been reported on throughout this paper and will simply be referred to as "broadband" data. The digital numbers of the broadband data are converted to radiance and at-satellite exo-atmospheric reflectance before being compared with narrowband data.

Digital Number to Radiance and At-Satellite Exatmospheric Reflectance
Broadband digital counts are converted to at-satellite exo-atmospheric reflectances using the following procedure. Mean Landsat-5 TM digital numbers from the 3- by 3-pixel locations were first converted to spectral radiance (Price, 1987) using the equation

$$R_i = \alpha_i \, DN_i + \beta_i \tag{1}$$

where R_i is the spectral radiance in mW cm^{-2}sr$^{-1}\mu$m^{-1}, α_i is the gain or slope in mW cm^{-2}sr$^{-1}\mu$m^{-1}, β_i is the bias or intercept in mW cm^{-2}sr$^{-1}\mu$m^{-1}, and DN_i is the digital number of each pixel or mean of a number of pixels in TM bands, where $i = 1$ to 5 and 7 (except the thermal band 6).

The effective at-satellite apparent reflectance or exo-atmospheric reflectance (ρ_p-unitless) is calculated using the equation

$$\rho_p = \pi R_i d^2 / \cos(\theta) * F_0 \tag{2}$$

where spectral radiance (R_i) is given by Equation 1, the Earth-sun distance (d) is expressed in astronomical units (A$_u$), θ is the solar zenith angle (which is 90 degrees minus the sun elevation or sun angle when the scene was recorded as given in the image header file), and F_0 is the solar flux or exatmospheric irradiances (Markam and Barker, 1985; Markam and Barker, 1987). This provides the nadir reflectance from both the surface and the atmosphere above it and normalizes the effects of solar elevation and Earth-sun distance. This is also referred to in the literature variously as planetary albedo or exatmospheric reflectance.

Broadband vegetation indices are computed using at-satellite exo-atmospheric reflectances.

Ground-Truth Data
The crop biophysical and yield data were obtained from 196 locations during April and May 1998 when most crops were in critical, or tillering, or late vegetative growth phases. The major crops were (Figure 1) barley (*Hordeum vulgare L.*; sample size 44), wheat (*Triticum aestivum L.* or *Triticum durum Desf.*; 64), lentil (*Lens esculenta Moench.* or *Lens orientale (Boiss.) Schmalh.* or *Lens culinaris Medikus*; 23), cumin (*Cuminum*

cyminum L.; 17), chickpea (*Cicer arietinum L.*; 14), and vetch (*Vicia narbonensis L.*; 14). Measurements were also taken from marginal lands (20) and fallow farms or top soils (9).

A representative sample area in each farm field was determined by the ground-truth team by observing the farm, choosing a representative plot area within the farm, and then throwing the 34- by 34-cm wooden block for a random location within the representative plot. Above-ground plant samples within a 34- by 34-cm (1156 cm²) wooden block were chosen for laboratory analysis. In the laboratory, plant samples were analyzed for leaf area (m²), wet weight (kilograms), dry weight (kilograms), and plant nitrogen content (percent). Leaf area was obtained by running the leaves over a LI-COR 3100 leaf area meter. The leaf area (cm²) obtained from plants in a representative area of 1156 cm² of farmland was converted into leaf area index (m²/m²). Plants were cut and weighed on a simple weighing machine to obtain the weight per 1156 cm². This weight was converted into biomass (kg/m²). Crop yield was obtained only for selected wheat farms by determining the after-harvest actual yield measurements (tonnes per hectare). Above ground plant height (PLNTHT) was measured directly in the field. Each plant sample was dried in an oven at 70°C, and dry weights were measured and then converted into dry biomass (kg/m²). The dried plants were crushed and assessed for plant crued protein (percentage) and nitrogen (percentage) for all crops and marginal lands. The mean nitrogen content (in percent) was Vetch (3.24), lentil (2.7), wheat (1.66), barley (1.17), chickpea (3.01), cumin (3.13), and marginal lands (1.45). The canopy cover was estimated by eye, separately by two field scientists. The mean canopy cover (in percent) was then calculated to be vetch (88), lentil (90), wheat (97), barley (97), chickpea (69), cumin (48), and marginal lands (68).

Hyperspectral and Multispectral Vegetation Indices
There is no single best approach for determining the optimal number of narrow wavebands required to provide best estimates of agricultural crop characteristics. In the past, researchers have used reflectance from individual narrowbands (Mariotti *et al.*, 1996), various ratio indices (Aoki, 1981; Carter, 1994; Lichtenthaler *et al.*, 1996; Lyon *et al.*, 1998), derivatives of reflectance spectra (Curran *et al.*, 1991; Elvide and Chen, 1995) or a combinations of these (Thenkabail *et al.*, 1999), principal component analysis (Clevers, 1999; Asner *et al.*, 2000; Thenkabail, 2002), discriminant analysis (Vaesen *et al.*, 2001; Thenkabail, 2002), and the linear mixture modeling approach (Elmore *et al.*, 2000; Mass, 2000). The focus in this paper will be to conduct a rigorous evaluation of narrowband versions of (1) two-band vegetation indices (TBVI) and (2) optimum multiple-band vegetation indices (OMBVI) in establishing relationships with agricultural crop growth and yield characteristics. Broadband versions of TBVI and OMBVI as well as six other broadband indices and their narrowband versions were computed, discussed, and compared with TBVI and OMBVI.

Two-Band Vegetation Indices (TBVI) (Thenkabail et al., 2000b; this paper)
The TBVI for narrow bands *i* and *j* will be

$$TBVI_{ij} = (R_j - R_i)/(R_j + R_i) \tag{3}$$

where $i, j = 1, ..., N$, where N is the number of narrow bands, i.e., 430 (each 1.43-nm-wide band spread over 395 nm to 1010 nm), and R is the reflectance of the narrow bands. Availability of hyperspectral data in 430 (N) discrete narrow wavebands facilitates the computation of $N \times N = 184,900$ narrow-waveband NDVIs for any one crop variable. In comparison, the seven Landsat TM bands have just 49 (7×7) possible indices. However, it will suffice to calculate narrow-waveband NDVIs only below the diagonal of the 430 by 430 matrix, because values
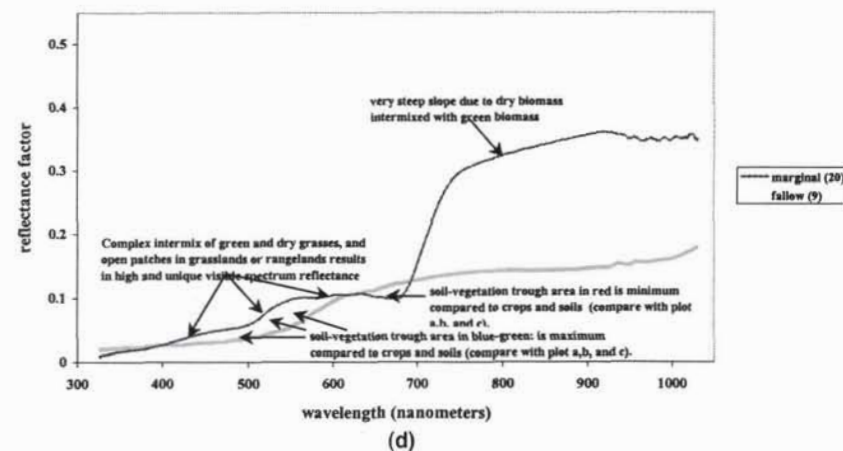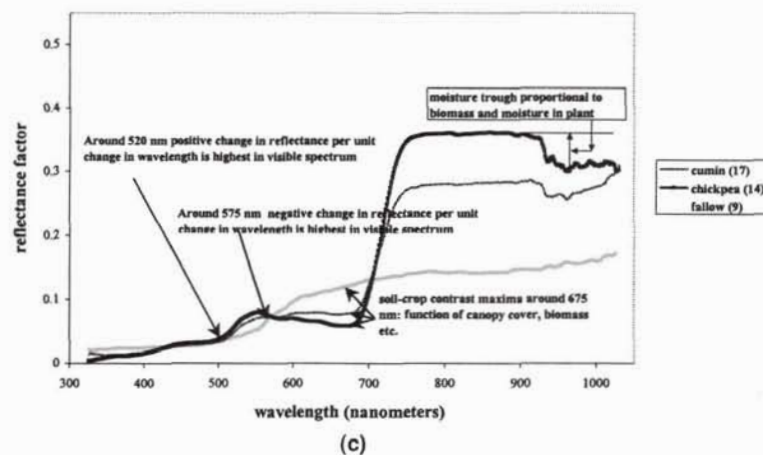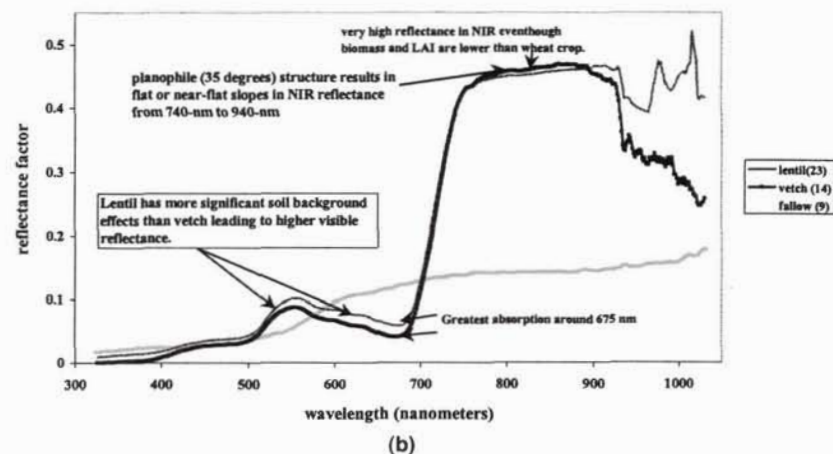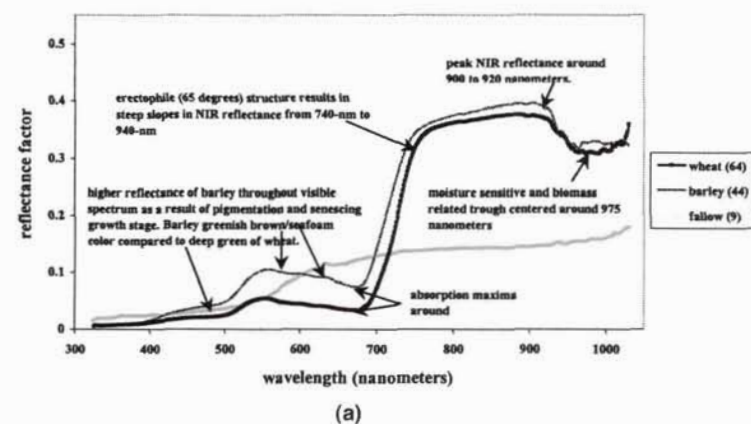
Figure 1. Average spectral characteristics of six crops and marginal lands. Figure shows (a) wheat and barley, (b) lentil and vetch, (c) chickpea and cumin, and (d) marginal lands. Spectral profiles of fallow farms are shown in all four plots.

above the diagonal are the transpose of values below the diagonal. All computations were performed by writing simple NDVI algorithms for all possible combinations of two-band indices using the Statistical Analysis System (SAS, 1997a; SAS, 1997b).

Broadband versions of TBVI were computed from Equation 3 using data from the six non-thermal Landsat-5 TM bands. Aggregating discrete narrowband data over the required bandwidths can also derive broadband data. The narrowband and broadband TBVIs were then related to crop biophysical variables using the SAS (SAS, 1997a; SAS, 1997b). Linear or non-linear models were fitted based on the plot trends and best-fit R^2 values.

Optimum Multiple-Band Vegetation Indices (OMBVI) (Thenkabail et al., 2000b; this paper)

The narrowband and broadband versions of OMBVI were computed using the following model equation:

$$\text{OMBVI}_i = \sum_{j=1}^{N} a_{ij}R_j \qquad (4)$$

where OMBVI$_i$ is the crop variable i, R_j is the reflectance in bands j ($j = 1$ to N with $N = 430$), and a_{ij} is the coefficient for reflectance in band j for the crop variable i. Of several statistical methods available to run piecewise linear regression models, the stepwise MAXR procedure is considered the best (SAS, 1997a; 1997b) and hence was used in this study. The MAXR method begins by finding the variable (R_j) producing the highest coefficient of determination (R^2) value (SAS, 1997a; SAS, 1997b). Then another variable, the one that yields the greatest increase in R^2 value, is added. Once the two-variable model is obtained, each of the variables in the model are compared to each variable not in the model. For each comparison, MAXR determines if removing one variable and replacing it with the other variable increases R^2. After comparing all possible choices, the one that produces the largest increase in R^2 is made. Comparisons begin again, and the process continues until MAXR finds that no replacement could increase R^2. The two-variable model thus achieved is considered the best two-variable model. Another variable is then added to the model, and the comparing-and-switching process is repeated to find the best three-variable model, and so forth (SAS, 1997a; SAS, 1997b) until the best n-variable model is determined.

NIR- and Red-Based Normalized Difference Vegetation Indices (NDVI) (Rouse et al., 1973; Jackson, 1983)

The NDVI is computed using the following equation:

$$\text{NDVI} = (\text{NIR} - \text{RED})/(\text{NIR} + \text{RED}) \qquad (5)$$

where, for broad bands (Landsat-5 TM): RED (TM3): 630 to 690 nanometers, NIR (TM4): 760 to 900 nm and, for narrow-bands (hyperspectral): RED ($\lambda_1 = 675$ nm): 668 to 683 nanometers ($\Delta\lambda_1 = 15$ nm), NIR ($\lambda_2 = 905$ nm): 898 to 913 nm ($\Delta\lambda_2 = 15$ nm); where λ_1 is the band center and $\Delta\lambda_1$ is the bandwidth. Preliminary studies indicated a narrow bandwidth of about 15 nm to be optimal in NIR and RED and was hence chosen.

Transformed Soil Adjusted Vegetation Indices (TSAVI) (Baret et al., 1989)

The TSAVI is computed using the following equation:

$$\text{TSAVI} = a^*(\text{NIR} - a^*\text{RED} - b)/(\text{RED} + a^*\text{NIR} - a^*b) \qquad (6)$$

where a is the slope and b is the intercept of soil lines. Forty-three spectral measurements of soils were taken using the Spectroradiometer at the topsoil. The slopes (a) and intercepts

(b) of the soil lines were computed by plotting mean reflectances for broadbands and narrowbands using RED and NIR bandwidths as provided for in Equation 5 above. These are fitted using the equation NIR = a^* RED + b.

Atmospherically Resistant Vegetation Indices (ARVI) (Kaufman and Tanre, 1992)

The ARVI is computed using the following equation:

$$\text{ARVI} = (\text{NIR} - \text{rb})/(\text{NIR} + \text{rb}) \qquad (7)$$

where rb = RED $-$ gamma $*$ (RED $-$ BLUE) and in which gamma = 1 and BLUE = TM1. It was not necessary to compute ARVI for narrowbands because atmospheric effects were not significant for hyperspectral measurements made at ground level.

Middle Infrared-Based Vegetation Indices (MIVI) (Thenkabail et al., 1995)

The MIVI is computed using the following equation:

$$\text{MIVI} = (\text{MIR1} - \text{RED})/(\text{MIR1} + \text{RED}) \qquad (8)$$

where MIR1 (TM5): 1550 to 1750 nm. TM5 provided the most information on crop growth and yield in a study of corn and soybeans (Thenkabail et al., 1994; Thenkabail et al., 1995). Therefore, an NDVI involving TM5 was selected. The hyperspectral observations were only in the visible and NIR and, hence, MIVI was computed only for broadbands.

Tassel-Cap-Based Greenness Vegetation Indices (TCGVI) (Jackson, 1983)

The Gram-Schmidt process (Jackson, 1983) was used to compute n-dimensional indices. The second component will provide TCGVI. Tassel cap equations were computed using the six non-thermal bands of the Landsat-5 TM image of 05 April 1998 covering the study area. TCGVI was not computed for narrowbands because it was beyond the scope of this paper.

Wetness (first component)

$$\text{TCWVI} = \text{TM1}^*0.2909 - \text{TM2}^*0.2728 + \text{TM3}^*0.1446$$
$$+ \text{TM4}^*0.8461 + \text{TM5}^*0.0549 + \text{TM7}^*0.1706$$

Greenness (GVI) (second component)

$$\text{TCGVI} = -\text{TM1}^*0.2728 - \text{TM2}^*0.2174 - \text{TM3}^*0.5508$$
$$+ \text{TM4}^*0.7221 + \text{TM5}^*0.0733 - \text{TM7}^*0.1648 \qquad (9)$$

Brightness (third component)

$$\text{TCBVI} = \text{TM1}^*0.1446 + \text{TM2}^*0.1761 + \text{TM3}^*0.3322$$
$$+ \text{TM4}^*0.3396 - \text{TM5}^*0.6210 - \text{TM7}^*0.4186$$

Principal Component Vegetation Indices (PCVI) (this paper)

Principal components analysis (Jensen, 1986) was used to reduce many bands of broadband and narrowband data to a few bands. Each principal component is computed using factor loadings and band values. The first two components explained between 86 and 96 percent of all variability in TM and hyperspectral data (Thenkabail, 2002). Using the weightings of the first principal component, new principal component band 1 brightness values (PCA1BV) are calculated. Similarly, using the weightings of the second principal component, new principal component band 2 brightness values (PCA2BV) are calculated. For example, digital numbers of six TM bands for field number 112 (barley crop) were 57, 24, 24, 73, 52, and 18. The PCA1 coefficients were -0.0564, 0.42323, 0.4455, 0.44708, 0.45723, and 0.45857. Therefore, the new brightness value, PCA1BV, for barley field number 112 will be 82.3019. Using the new principal

component bands 1 and 2, a principal component vegetation index was computed: i.e.,

$$PCVI = (PCA1BV - PCA2BV)/(PAC1BV + PCA2BV). \quad (10)$$

Results and Discussions

Spectral Characteristics

Mean spectral plots of six agricultural crops, marginal lands, and soils illustrate several unique plant characteristics at specific portions of the spectrum (see Figures 1a through 1d). The cereal crops (wheat and barley) had erectophile (about 65 degrees) structure resulting in a steep slope in the near-infrared (NIR) spectra as seen in the 740- to 940-nanometer range (Figure 1a). Reflectivity in the visible spectrum range of 450 to 700 nm was dramatically different for wheat when compared with barley (Figure 1a). This was due to growth stage differences with critical growth phases for wheat when compared to senescing for barley. As on 06 April 1998 (date of acquisition of the image), wheat was greener than barley. Barley was senescing and was a mixture of brown and green, resulting in dramatically higher visible reflectance for barley when compared with wheat. Two of the legumes, lentil and vetch, had very high NIR reflectance and very high red absorption (Figure 1b). There are number of reasons for this. The lentil and vetch are in late vegetative vigorous growth phases with mean canopy cover of about 90 percent. Both are nitrogen fixation crops with a relatively high plant nitrogen content of 3.24 percent for vetch and 2.70 percent for lentil. Compared to legumes, the plant nitrogen in wheat (1.66 percent) and barley (1.17 percent) was significantly lower. Lentil, vetch, chickpea, and cumin are significantly shorter and greener than wheat or barley, which were in later phenological growth stages. Furthermore, the planophile structure of legumes (about 35 degrees) contributes to a near flat NIR reflectivity (referred to as NIR shoulder) in the 740- to 940-nanometer range. Soil background effects were significant for (1) cumin with only 48 percent mean canopy cover, and (2) chickpea with 69 percent canopy cover. This resulted in relatively low NIR reflectance and high visible reflectance for these crops (Figure 1c). Marginal lands were a mixture of various levels of green, and dry biomass. They often have significant barren patches and/or dry and green patches intermingled. These conditions resulted in steep NIR and visible reflectance slopes, a high degree of sensitivity in the red-edge (700 to 740 nm), higher reflectance in the visible, and a very mild "trough" in the 940- to 1010-nm moisture sensitive region (Figure 1d). In the 675- to 700-nm range, soil-crop contrast is significantly higher for healthy and vigorous crops (e.g., Figure 1b) when compared with crops or vegetation that are senescing (e.g., barley in Figure 1a) or with significant soil background effects (e.g., cumin or chickpea in Figure 1c) or with a mix of dry and green vegetation conditions (e.g., rangelands in Figure 1d).

In the following section, various vegetation indices are computed from the reflectance spectra. Broadband and narrowband versions of the best two-band NDVI-type vegetation indices (TBVI) and optimum multiple-band vegetation indices (OMBVI) were computed and compared with six other types of vegetation indices (NDVI, TSAVI, ARVI, MIVI, TCGVI, and PCVI).

Narrowband and Broadband TBVI and Crop Variables

The relationships between narrowband and broadband TBVI with crop biophysical variables (wet biomass-WBM, dry biomass-DBM, leaf area index-LAI, and plant height-PLNTHT) were established and their coefficient of determination (R^2) was determined for the six crops (Table 2). TBVI was also related to plant nitrogen and canopy cover, but these relationships were generally not as strong as with WBM, DBM, LAI, and PLNTHT. Hence, results with plant nitrogen and canopy cover will not be reported. Relationships were also established for wet and

dry biomass of marginal lands (Table 2). A contour plot of the R^2 values for narrowband wavelength pairs λ_1 (430 bands in 395 to 1010 μm) and λ_2 (430 bands in 395 to 1010 μm) are plotted and illustrated for (1) LAI of barley (values below the diagonal in Plate 1) and (2) LAI of wheat (values above the diagonal in Plate 1). For a given crop variable, it will suffice to display the matrix only below (or above) the diagonal of the matrix because the R^2 values above and below the diagonal of the matrix are symmetrical. Only R^2 values above 0.4 are plotted for clarity. These plots show the waveband combinations that provide the best indices (see various "bulls-eye" formations in Plate 1) for relationships with crop biophysical variables. For example, waveband centers for the best TBVI index for barley LAI were 720 nm and 815 nm, providing R^2 in the range of 0.76 to 0.79 (Plate 1) with the precise R^2 value of the best index being 0.79 (Table 2). Similarly, the best estimates of wheat LAI were obtained using two narrowbands centered at 680 nm and 910 nm (Plate 1), providing an R^2 value of 0.74 (Table 2). Similar λ_1 versus λ_2 plots were used to determine the best waveband combinations that estimated other biophysical variables of the six crops and marginal lands (Table 2). Also computed were the best possible combinations of Landsat-5 TM broadband TBVI indices (Table 2).

Narrowband TBVI indices consistently performed better than their broadband versions by explaining one to 24 percent greater variability (with a mean of about 10 percent) in determining various crop variables (Table 2). Generic relationships involving multiple crops that have a wide range of growing stages, growing conditions, and background effects are used to illustrate this. Compared to broadband relationships with biophysical quantities (Figures 2a and 2b), the narrowband relationships (Figures 2c and 2d) provide significantly better results because of their greater sensitivity to plant pigmentation, canopy structure, and soil background effects, and their greater robustness to a complex mix of growing conditions and growth stages. As a result, the dynamic range of narrowband indices (Figures 2c and 2d) is better than the broadband indices (Figures 2a and 2b). In general, one or more narrowband indices provide greater dynamic range and are more robust in accounting for variability in a wide range of conditions such as soil background effects, growth stages, and pigmentation levels, result-ing in significantly improved R^2 values compared to the best broadband Landsat-5 TM indices. It should be noted that broadband data stretches from 450 nm to 2350 nm (nonthermal TM bands) and include mid-infrared bands (TM5 and TM7), where-as the narrowband data were acquired only at 395 to 1010 nm. Therefore, the narrowband results are even more significant.

Optimal narrowband bandwidths were determined from the λ_1 versus λ_2 plots (e.g., Plate 1) by observing the change in R^2 value from the band centers. For example, for barley LAI, along λ_1 the value of R^2 remains constant from about 750 nm to 880 nm with the center at 815 nm, resulting in a $\Delta\lambda_1 = 130$ nm (Plate 1). However, along λ_2 the value of R^2 remains constant only for a very narrow width of about 10 nm ($\Delta\lambda_2$) with center at 720 nm (Plate 1). The bandwidths were rounded off to the nearest 5s or 10s (e.g., 8.5 nm is rounded off to 10 nm). For wheat LAI (Plate 1), both the λ_1 (680 nm) and λ_2 (910 nm) have a narrowband width of about 20 nm ($\Delta\lambda_1 = \Delta\lambda_2$) with an R^2 value of 0.74. The best NIR- and red-based narrowband indices can be computed by taking a (1) very narrowband centered around 675 nm ($\Delta\lambda = 15$ nm) for red and (2) narrowband centered around 905 nm or 920 nm ($\Delta\lambda = 15$ nm) for NIR.

Optimum Multiple-Band Vegetation Indices (OMBVI) and Crop Variables

Using the MAXR procedure of SAS (1997), the best one-variable, two-variable, and three-variable OMBVI models were determined for estimating wet biomass, dry biomass, leaf area index, and plant height of six crops (Table 3). The best one-variable

TABLE 2. WAVEBANDS CENTERS AND R^2 VALUES FOR BEST TBVI MODELS. THE TWO-BAND VEGETATION INDICES (TBVIs) PROVIDING R^2 VALUES FOR THE BEST MODELS USED IN ESTIMATING VARIOUS BIOPHYSICAL VARIABLES

Crop	Variable	Landsat-5 TM data				Hyperspectral data						Increased variability explained by the best hyperspectral index when compared with the best Landsat-5 TM index (percent)
		Best index		Second best index		Best index		Second best index		Third best index		
		Spectral band centers in NDVI-type index	R^2	Spectral band centers in NDVI-type index R^2	R^2	spectral band centers in NDVI-type index	R^2	spectral band centers in NDVI-type index	R^2	spectral band centers in NDVI-type index	R^2	
1. Barley[A] (44)	WBM	TM3,TM4	0.75	TM2,TM3	0.69	675,820	0.84	495,525	0.80	455,840	0.78	9
	DBM	TM3,TM4	0.76	TM2,TM4	0.65	670,910	0.81	675,760	0.80	550,568	0.75	5
	LAI	TM3,TM4	0.71	TM2,TM3	0.62	720,815	0.79	675,700	0.76	550,590	0.73	8
	PLNTHT	TM2,TM3	0.44	TM3,TM4	0.40	670,905	0.45	675,575	0.43	410,920	0.40	1
2. Wheat[A] (64)	WBM	TM2,TM4	0.70	TM2,TM4	0.67	604,904	0.83	590,845	0.81	550,590	0.61	13
	DBM	TM3,TM4	0.65	TM2,TM4	0.64	545,910	0.80	700,910	0.79	550,830	0.74	15
	LAI	TM2,TM4	0.66	TM2,TM4	0.66	680,910	0.74	515,910	0.73	635,880	0.72	8
	PLNTHT	TM3,TM4	0.37	TM2,TM4	0.36	437,880	0.41	550,880	0.39	715,860	0.34	4
3. Lentil[A] (23)	WBM	TM3,TM4	0.80	TM2,TM3	0.74	675,910	0.85	418,904	0.82	550,675	0.81	5
	DBM	TM3,TM4	0.68	TM2,TM4	0.64	675,845	0.78	675,985	0.75	550,678	0.73	10
	LAI	TM3,TM4	0.78	TM1,TM3	0.71	670,845	0.84	445,905	0.84	675,975	0.81	6
	PLNTHT	TM1,TM3	0.26	TM3,TM4	0.24	675,910	0.50	680,980	0.49	646,680	0.48	24
4. Cumin[B] (17)	WBM	TM2,TM4	0.75	TM2,TM3	0.69	678,880	0.80	568,675	0.79	678,920	0.75	5
	DBM	TM2,TM4	0.71	TM2,TM4	0.67	675,800	0.87	568,678	0.81	495,880	0.78	20
	LAI	TM3,TM4	0.70	TM1,TM3	0.64	568,661	0.85	678,775	0.83	490,845	0.83	15
	PLNTHT	TM3,TM7	0.15	TM3,TM4	0.06		NS		NS		NS	NA
5. Chickpea[A] (14)	WBM	TM3,TM4	0.86	TM2,TM4	0.79	568,678	0.95	670,810	0.95	495,820	0.94	9
	DBM	TM3,TM4	0.72	TM2,TM3	0.68	750,965	0.91	760,775	0.91	535,620	0.89	21
	LAI	TM3,TM4	0.78	TM2,TM3	0.71	720,840	0.92	495,840	0.91	550,680	0.89	14
	PLNTHT	TM3,TM4	0.83	TM5,TM7	0.79	690,840	0.96	550,680	0.95	495,845	0.93	8
6. Vetch[B] (14)	WBM	TM3,TM5	0.74	TM3,TM4	0.73	675,820	0.82	418,661	0.70	520,604	0.63	8
	DBM	TM3,TM5	0.72	TM2,TM4	0.65	715,910	0.84	550,880	0.72	525,575	0.67	11
	LAI	TM3,TM5	0.77	TM3,TM4	0.65	720,910	0.80	568,910	0.68	460,920	0.64	3
	PLNTHT	TM1,TM5	0.11	TM5,TM7	0.11	668,682	0.24	965,982	0.28	765,965	0.13	13
7. Marginal[A] (20)	WBM	TM2,TM3	0.87	TM3,TM4	0.83	672,906	0.89	568,675	0.80	418,525	0.77	2
	DBM	TM2,TM3	0.78	TM1,TM3	0.82	680,908	0.80	437,910	0.76	550,682	0.69	2

Note: A = Non-linear exponential models of the type $Y = a*e^{b*x}$; B = Linear models of the type $Y = a + b * x$. NS = not significant, NA = not available.
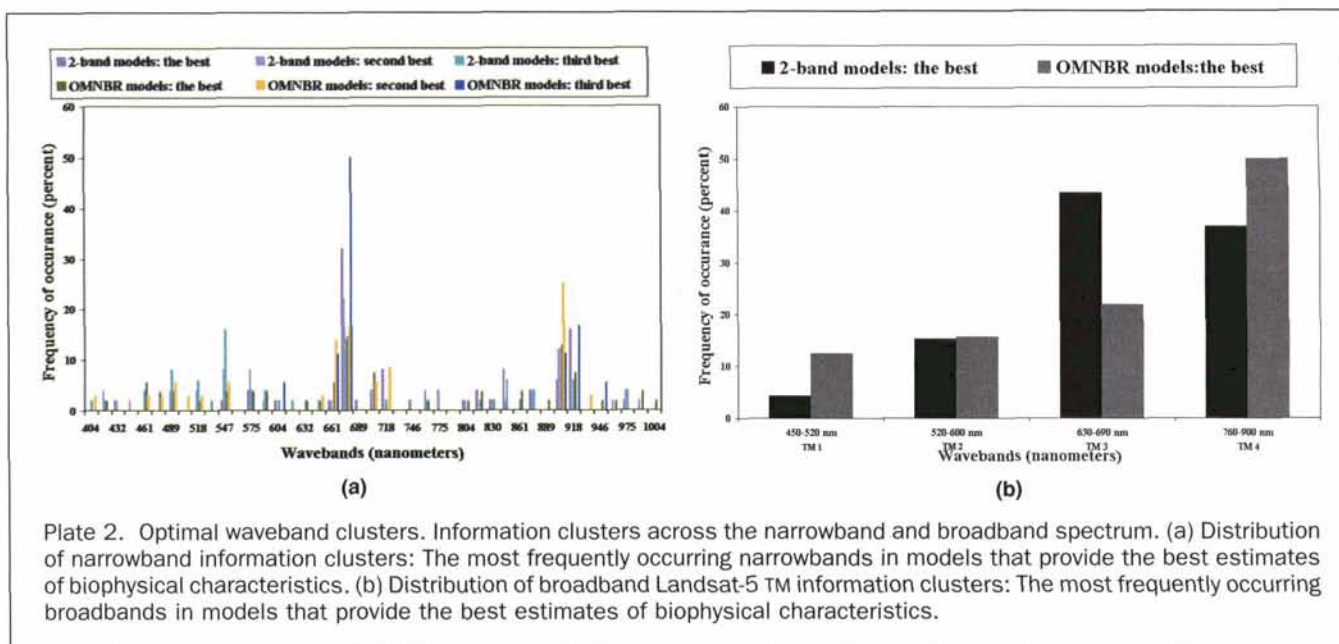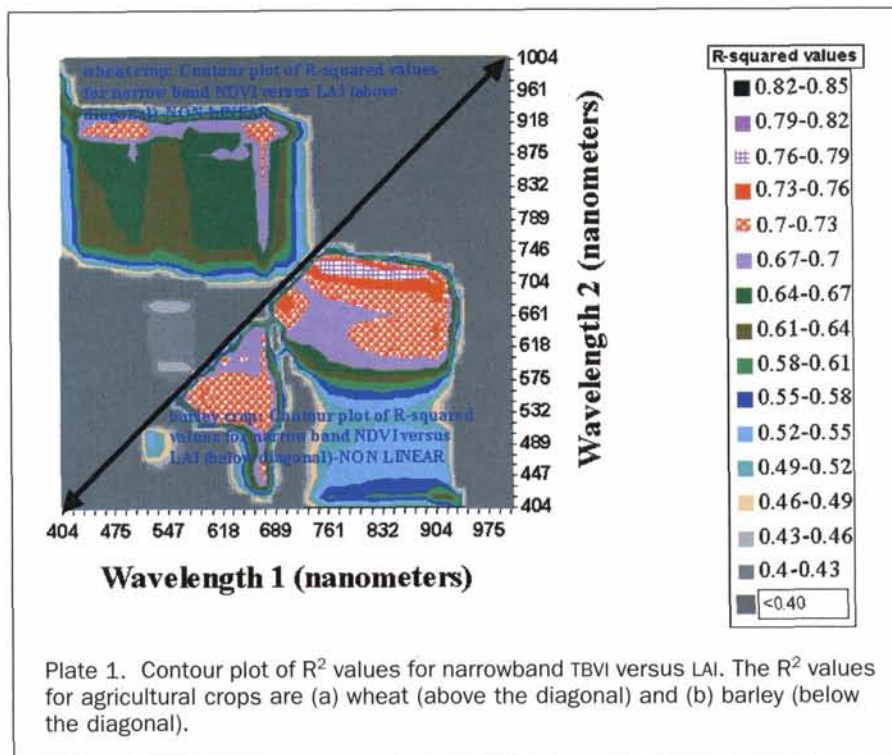
narrowband model explained 38 to 94 percent of variability across different crop variables (Table 3). This increased to 56 to 98 percent for best two-variable models and 60 to 99 percent for the best three-variable models. In an overwhelming number of cases, further addition of independent variables only increased R^2 values insignificantly. Hence, three bands are considered optimal. The addition of a third band often helps overcome the problem of saturation associated with two-band NDVI type indices. However, the problem of "over fitting" (e.g., using more spectral channels than experimental samples to obtain a perfect R^2 value) needs to be avoided while using OMBVI models (see Blackburn (1998) and Thenkabail et al. (2000b)). In comparison, the best two or three Landsat-5 TM broadband OMBVI indices explained 60 to 89 percent of crop variability (Table 3). Overall, the narrowband OMBVI indices explained 1 to 27 percent greater variability than did the broadband OMBVI indices. In estimating cumin LAI, the best three-variable narrowband OMBVI indices explained 22 percent greater variability when compared with the best broadband NDVI indices (Table 3). With only 48 percent canopy cover, cumin is subjected to significant soil background effects that are well modeled using narrowbands centered at 589 nm, 675 nm, and 904 nm, whereas the best broadbands fail to capture this variability (Table 3).

The narrowband OMBVI (Table 3) performed better than narrowband TBVI (Table 2) nine times, poorer eight times, and was equal once (Table 3). The results demonstrate that some combination of two or three bands provides the best estimates of crop biophysical variables. The sensitivity of any particular portion of a waveband is a function of crop conditions, growth stages, and numerous other factors such as irrigation and soil types. Hence, different combinations of bands provide the best results (Table 2 and Table 3). For example, the soil background effects were significant in cumin (48 percent canopy cover) and chickpea (69 percent) compared to wheat (97 percent) or barley (97 percent). It is, therefore, interesting to note that an addition of a third band in OMBVI indices improves R^2 values by 4 to 12 percent in WBM and LAI of cumin and chickpea compared to their best two-band TBVIs (Table 4). By contrast, when soil background is insignificant, as in case of wheat and barley, addition of a third band is not of importance with three of the four models (WBM of barley, WBM and LAI of wheat; Table 4) showing better R^2 values for two-band TBVI over three-band OMBVI.

Comparison of TBVI and OMBVI with Various other Vegetation Indices

Relationships of six other unique narrowband and broadband vegetation indices were established with wet biomass (WBM) and leaf area index (LAI) of six crops and compared with the narrowband and broadband TBVI and OMBVI (Table 4). In 11 of the 12 crop models, the best indices were narrowband versions of either OMBVI or TBVI (see Table 4). The two-band vegetation index (TBVI) uses the best two narrowband or broadband combinations compared to NDVI, which rigidly uses a NIR and a red band. As a result, there is a significant improvement in estimates of several crop variables using TBVI when compared with NDVI. For example, cumin WBM and LAI (Table 4). NDVI is based on the contrast of high reflectance in the NIR and high absorption in the red. NDVI normalizes the topographic effects, is sensitive to photosynthetically active radiation, is a simple and reliable measure of greenness in remotely sensed data for a

Plate 1. Contour plot of R² values for narrowband TBVI versus LAI. The R² values for agricultural crops are (a) wheat (above the diagonal) and (b) barley (below the diagonal).

Plate 2. Optimal waveband clusters. Information clusters across the narrowband and broadband spectrum. (a) Distribution of narrowband information clusters: The most frequently occurring narrowbands in models that provide the best estimates of biophysical characteristics. (b) Distribution of broadband Landsat-5 TM information clusters: The most frequently occurring broadbands in models that provide the best estimates of biophysical characteristics.

single date, and is conveniently scaled between −1 and +1 (Lyon *et al.*, 1998). However, NDVI often overestimates vegetation in darker soils compared to brighter soils (Elvidge and Lyon, 1985).

The transformed soil adjusted index (TSAVI) serves to reduce the variance associated with soil background influences, but does not enhance the variance of the vegetation canopy reflectances. TSAVI is expected to account for local changes in soil color, texture, and brightness (Huete, 1988; Baret *et al.*, 1989; Qi *et al.*, 1994) and is among the most sensitive vegetation indices (Lawrence and Ripple, 1998). Overall, R² values for TSAVI were significantly lower than those of the TBVI or OMBVI

models (Table 4). It appears that the normalization of the soil background influences to a constant ratio or a perfect one-dimensional soil line only removes bare soil spectral influences and not the greater soil brightness influences (Huete *et al.*, 1985). The performance of TSAVI is dependant on a precise estimate of the local soil line. In this study, the soil line was determined using soil reflectance data from 43 locations. Gathering soil reflectance data from each sample site location in real time requires a more precise estimate of soil line. Soil line is a function of so many variables (e.g., texture, color, organic content) that needs to be accounted for in order to obtain a perfect soil line. Furthermore, the micro conditions vary even
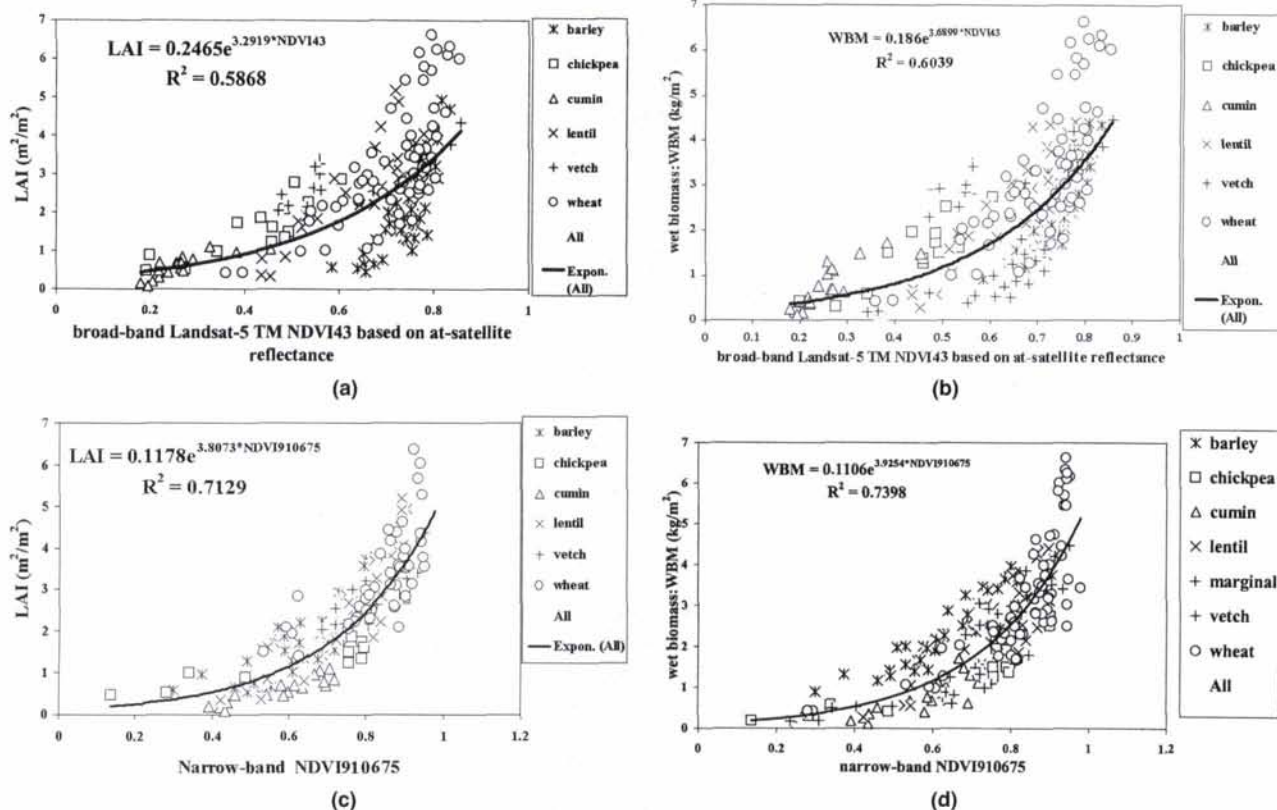
Figure 2. Broadband and narrowband indices versus crop biophysical variables. Relationship of broadband Landsat-5 TM NDVI of all six crops with (a) LAI and (b) wet biomass compared with two-band vegetation indices (TBVI) of narrowbands of all six crops with (c) LAI and (d) wet biomass.

within a field (e.g., moisture-rainfall, irrigation, tillage, drainage, slopes) that also needs to be accounted for. It appears that accounting for the micro variability in soil at each sample site location may be needed in order to better assess TSAVI.

The broadband atmospherically resistant indices (ARVI) are computed only for atmospherically effected Landsat-5 TM data; hence, the discussion is limited to broadband indices only. Generally, ARVIs, perform slightly better than do the broadband NDVI or TSAVI (Table 4). ARVI serve to reduce variance associated with atmospheric influences, not to enhance the variance of the vegetation canopy reflectances. The results indicate a marginal improvement with atmospheric correction in the majority of models. However, it needs to be noted that the ARVI was corrected only for atmospheric scattering and not for atmospheric absorption, for which time and location specific climatic data are needed, which are often difficult to obtain.

A significant proportion of the best three-variable Landsat-5 broadband indices (Table 3) consists of the mid-infrared bands (TM5 and TM7), indicating the importance of these bands in establishing crop characteristics. Mid-infrared bands provide valuable complementary information about the geometric structure of canopies, on optical properties of underlying soils (Boyd and Ripple, 1997; Boyd et al., 1999), and in handling complex dissimilar growth stages and growing conditions (Thenkabail et al., 1994; Thenkabail et al., 1995).

The tasseled-cap-based greenness vegetation index, TCGVI, uses data from six non-thermal TM bands and yet explains less variability than do the two-band TBVI or multiband OMBVI or red- and NIR-based NDVI (Table 4). Similarly, broadband and narrowband PCVI (Table 4), computed using principal-compo-

nent-derived wavebands 1 and 2, performed poorer than did NDVI, TBVI, or OMBVI. The coefficients of TCGVI and PCVI were computed from the TM image of the entire study area. Apart from the six agricultural crops and rangelands used in this study, the study area consists of many other crops in varying growth stages, agroforests, several other vegetation types, and land-cover types. As a result, the coefficients in TCGVI or PCVI are generalized and are less effective for specific crops. However, TCGVI or PCVI might provide equations that are more robust across crops and for a composite mix of vegetations.

Model Evaluations

The strengths of the spectro-biophysical models were tested using independent datasets for wheat crops (Figure 3). For the 18 independent wheat fields (data not used in model development), there was a high degree of correlation ($R^2 = 0.89$) between actual and predicted wet biomass. The predicted wet biomass was calculated using the equation WBM = 01429 $e^{3.6287*NDVI920675}$. The NDVI920675 was computed using the best two narrowbands (based on model evaluations for all crops) that involved bands centered at 920 and 675 nanometers. A nominal bandwidth of 15 nanometers was used for each narrowband. Other crops had relatively smaller sample sizes (see Figure 1), requiring all data to be used for model development.

Optimal Number of Narrowbands, Band Centers, and Bandwidths

The frequency of occurrence of narrowbands in the best three TBVI models (Tables 2 and 3) and OMBVI models (Table 3) were determined and their distribution in the visible and near-infrared spectrum were plotted (Plate 2a). An overwhelming pro-

TABLE 3. WAVEBANDS CENTERS AND R^2 VALUES FOR BEST OMBVI MODELS. THE OPTIMUM MULTIPLE-BAND VEGETATION INDICES (OMBVI'S) PROVIDING R^2 VALUES FOR THE BEST MODELS USED IN ESTIMATING VARIOUS BIOPHYSICAL VARIABLES[AA,BB]

| Crop type (sample size) | Dependant crop variable | Hyperspectral Data | | | | | | Landsat TM Data | | Best R^2 value for two-band normalized difference vegetation index models (these results from Table 4) | | Percent increase in best three-variable (OMNBR) model over: | |
| | | Best one-variable model OMNBR (best one-variable models) | | Best two-variable model OMNBR (best two-variable models) | | Best three-variable model OMNBR (best three-variable models) | | Best two- or three-variable model OMNBR (best three-variable models) | | | | | |
		Band centers (nm)[CC] (independent variable)	R^2 value	Band centers (nm)[CC] (independent variables)	R^2 value	Band centers (nm)[CC] (independent variables)	R^2 value	TM bands (independent variables)	R^2 value	Broad-band Landsat TM NDVI model R^2	Narrow-band spectro NDVI model R^2	Broad-band NDVI	Narrow-band NDVI
1. Barley (44)	WBM	675	0.56	675,904	0.77	418,675,904	0.80	TM3, TM4	0.68	0.75	**0.84**	+5	−4
	DBM	675	0.49	646,718	0.77	461,632,704	0.80	TM3, TM4	0.69	0.76	**0.81**	+4	−1
	LAI	675	0.44	704,904	0.77	704,904,989	**0.82**	TM3, TM4	0.64	0.71	0.79	+11	+3
2. Wheat (64)	WBM	904	0.49	518,904	0.74	518,575,904	0.76	TM2, TM4	0.60	0.70	**0.83**	+6	−7
	DBM	604	0.38	547,904	0.62	547,904,932	0.67	TM4, TM5	0.60	0.65	**0.80**	+2	−13
	LAI	675	0.41	718,904	0.56	704,904,918	0.60	TM3, TM4	0.60	0.66	0.74	−6	−14
3. Lentil (23)	WBM	675	0.65	675,904	0.76	646,804,918	0.82	TM3, TM4	0.82	0.80	**0.85**	+2	−3
	DBM	675	0.58	404,675	0.66	575,675,961	0.71	TM3, TM4, TM5	0.64	0.68	**0.78**	+3	−7
	LAI	675	0.70	475,547	0.83	461,475,541	**0.84**	TM2, TM4	0.79	0.78	**0.84**	+6	0
4. Cumin (17)	WBM	675	0.42	675,704	0.84	675,704,989	**0.89**	TM2, TM4	0.77	0.75	0.80	+14	+9
	DBM	661	0.59	489,661	0.83	675,761,804	**0.95**	TM2, TM4	0.82	0.71	0.87	+24	+8
	LAI	661	0.55	504,661	0.94	589,675,904	**0.92**	TM2, TM4	0.79	0.70	0.85	+22	+7
5. Chickpea (14)	WBM	904	0.87	661,675	0.98	461,661,675	**0.99**	TM1, TM4, TM7	0.89	0.86	0.95	+13	+4
	DBM	946	0.94	489,932	0.98	489,918,1004	**0.99**	TM1, TM5, TM7	0.74	0.72	0.91	+27	+8
	LAI	675	0.85	661,675	0.96	589,661,675	**0.97**	TM1, TM4, TM7	0.80	0.78	0.92	+19	+5
6. Vetch (14)	WBM	918	0.42	661,904	0.76	661,818,889	**0.85**	TM3, TM5	0.78	0.74	0.75	+11	+10
	DBM	918	0.45	718,904	0.82	675,818,861	**0.95**	TM4, TM5	0.76	0.72	0.84	+23	+11
	LAI	918	0.40	461,904	0.72	475,489,904	0.78	TM1, TM4	0.74	0.77	**0.80**	+1	−2

Note: AA = piecewise multiple linear narrow-band (OMNBR) models were obtained using MAXR algorithm in SAS (1997a; 1997b).

BB = The model with highest R^2 between OMNBR (three-variable), narrow-band NDVI, and broad-band NDVI is shown in bold;

CC = bandwidths are 1.43 nanometers wide for each band center. Band centers in decimal fractions were rounded off to the nearest whole number (e.g., 549.86 nanometers as 550 nanometers.
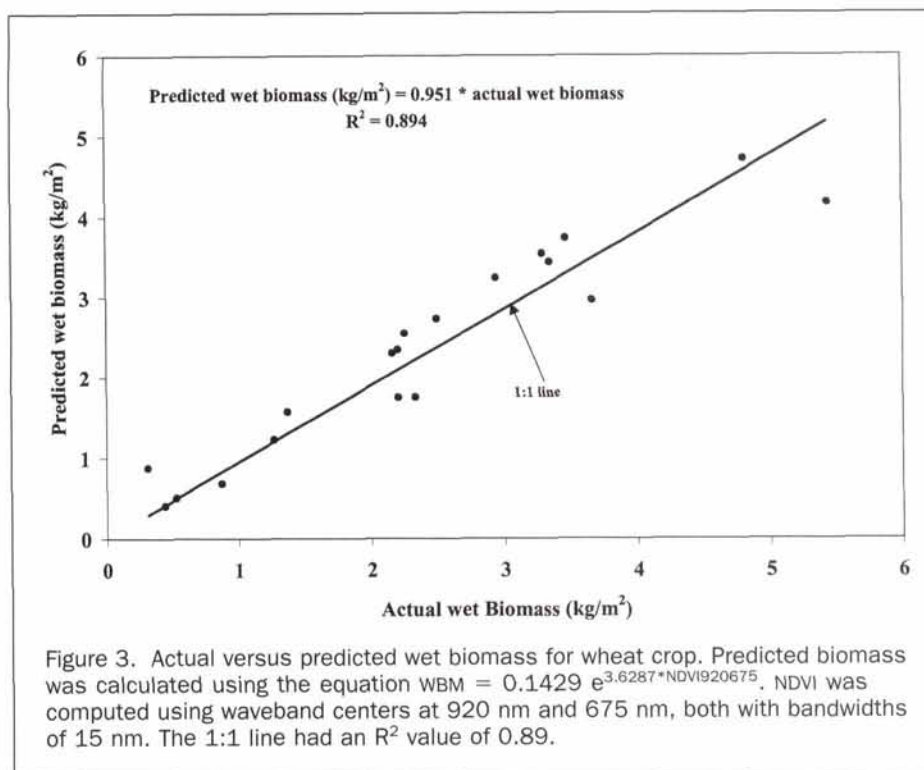
portion of crop information is concentrated in a few narrowbands. The four most prominent narrowbands are (Plate 2a) the red absorption maxima between 660 nm and 690 nm, the near-infrared reflection peak between 900 nm and 920 nm, a portion of the red-edge between 700 nm and 720 nm, and the green reflectance maxima centered between 540 nm and 560 nm. A more careful evaluation identified information clusters for 12 distinct narrowbands (Table 5). The 12 optimal narrowbands in the visible and NIR are one blue, three green, two red, two red-edge, one NIR, two NIR peak, and one NIR moisture sensitive. The bandwidths are defined as very narrow (less than or equal to 15 nanometers) or narrow (15 to 30 nm) or broad (greater than 30 nm). Based on this definition, only band 9 at 120 nm is broadband (Table 5). The other 11 bands are narrowbands (Table 5). The band centers and bandwidths presented in Table 5 are derived from the results of Tables 2, 3, and 4 and Plates such as 1 and 2. Bandwidths can be obtained from contour widths in Plate 1. The band centers and widths are rounded off to the nearest 5 nm or 10 nm (e.g., 718 nm as 720 nm). A number of these band centers are positioned where the soil (fallow farms) and vegetation slopes intersect and head in opposite directions (see Figures 1a through 1d), resulting in increased sensitivity of indices using this portion of the spectrum. For example, at 570 nm for chickpea and cumin (Figure 1c) and 720 nm for wheat (Figure 1a).

The two-band indices, TBVIs, that are the best can be formulated using narrowband combinations of a red and a NIR peak, or a red and a NIR "shoulder," or a red-edge and a NIR peak, or a red-edge and a NIR shoulder, or a green and a red band combinations (Tables 2 and 3). Bandwidths can vary from 5 nm to 30 nm (Table 5). Wavebands along the NIR "shoulder" can be either a broadband or a narrowband, providing similar results. For the three-variable multi-linear OMBVI models (Table 3), band combinations that provide the best results are, typically, combinations of any three narrowbands consisting of red, NIR peak, red-edge, blue, or green. In Landsat-5 TM a red (TM3) and a NIR (TM4) band provide the best results followed by the green (TM2) band (Plate 2b and Tables 2 and 4). Narrowband versions of these bands are (Table 5) band 6 ($\lambda = 675$ nm, $\Delta\lambda = 15$ nm), band 10 or 11 ($\lambda = 905$ or 920 nm, $\Delta\lambda = 15$ nm), and band 3 ($\lambda = 550$ nm, $\Delta\lambda = 25$ nm). For example, barley dry biomass was estimated with an R^2 value of 0.81 using narrowbands centered at 670 nm and 910 nm compared to a best R^2 value of 0.76 using broadbands TM3 and TM4 (Table 2). Common vegetation reflectance peaks at around 900 nm to 940 nm and absorption peaks around 670 nm or 690 nm (e.g., Figure 1). Results (Tables 2, 3, and 4 and Plate 2a) indicate that these wavebands provide maximum crop information. Earlier, Blackburn (1998; 1999) also found Chlorophyll a and b of crops or vegetation to be most strongly correlated around 670 nm and 680 nm. Elvidge and Chen (1995), Carter (1998), and Thenkabail (2000a) found wavebands in the range of 680 to 700 nm and 900 to 940 nm to be most sensitive to crop characteristics. Blackburn and Steele (1999) inferred broadbands to be far less sensitive to pigment concentrations, LAI, or percent cover relative to narrowbands. The structure of plant canopy has a significant bearing on spectral signature. For example, the planophile (30 degrees) structure of legumes such as vetch and lentil (Figure 1b) contribute to significantly greater reflectance in NIR and greater absorption in red when compared with erectophile (65 degrees) structure of cereals such as wheat and barley (Figure 1a). The erectophile structure leads to significant slope changes in spectra in the region of 740 nm to 940 nm (Figure 1a).

The above results further indicate that the optimal information on crops are not necessarily concentrated in the red and NIR wavelengths but are often in other portions of the wavebands such as red-edge or green or moisture sensitive NIR. For example, chickpea WBM is best modeled using two visible bands: a green band centered at 568 nm ($\Delta\lambda_1 = 10$) and a red

Table 4. TBVI and OMBVI Models Compared to Six Other VI Models. Evaluation of Eight Categories of Hyperspectral Narrowband and Multispectral Broadband Vegetation Indices

Crop type	Bio-physical variables	Best two-band vegetation index B2BVI Broad-Band Landsat TM	Best two-band vegetation index B2BVI Narrow-Band Hyperspectral	Optimum multiple band vegetation index OMBVI Broad-Band Landsat TM	Optimum multiple band vegetation index OMBVI Narrow-Band Hyperspectral	NIR- and red-based vegetation index NDVI Broad-Band Landsat TM	NIR- and red-based vegetation index NDVI Narrow-Band Hyperspectral	Transformed-soil-adjusted vegetation index TSAVI Broad-Band Landsat TM	Transformed-soil-adjusted vegetation index TSAVI Narrow-Band Hyperspectral	Atmospheric-corrected vegetation index ACVI Broad-Band Landsat TM	Atmospheric-corrected vegetation index ACVI Narrow-Band Hyperspectral	Middle-infrared-based vegetation index MIVI Broad-Band Landsat TM	Middle-infrared-based vegetation index MIVI Narrow-Band Hyperspectral	Tassel-cap-based greenness vegetation index TCGVI Broad-Band Landsat TM	Tassel-cap-based greenness vegetation index TCGVI Narrow-Band Hyperspectral	Principal-component-based vegetation index PCVI Broad-Band Landsat TM	Principal-component-based vegetation index PCVI Narrow-Band Hyperspectral
1. Barley	WBM	0.75	**0.84**	0.68	0.80	0.75	**0.84**	0.74	**0.84**	0.75		0.58		0.52		0.50	0.78
	LAI	0.70	0.79	0.64	0.82	0.63	0.79	0.72	0.73	0.68		0.65		0.54		0.56	0.77
2. Wheat	WBM	0.70	**0.83**	0.60	0.76	0.69	0.82	0.69	0.79	0.69	Atmospheric affect NOT significant	0.62	Mid-infrared data NOT available	0.63	Not computed	0.66	0.80
	LAI	0.66	**0.74**	0.60	0.60	0.59	0.72	0.65	0.73	0.71		0.55		0.61		0.59	0.70
3. Lentil	WBM	0.80	0.85	0.82	0.82	0.80	0.85	0.79	**0.86**	0.82		0.67		0.69		0.69	0.75
	LAI	0.78	**0.84**	0.79	**0.84**	0.78	0.84	0.77	0.83	0.79		0.66		0.66		0.65	0.79
4. Cumin	WBM	0.75	0.80	0.77	**0.89**	0.63	0.75	0.55	0.76	0.73	Atmospheric affect NOT significant.	0.62		0.65		0.49	0.61
	LAI	0.70	0.85	0.79	**0.97**	0.70	0.77	0.51	0.75	0.77		0.58		0.54		0.62	0.72
5. Chickpea	WBM	0.86	0.95	0.89	**0.99**	0.86	0.88	0.86	0.94	0.75		0.78		0.82		0.82	0.92
	LAI	0.78	0.92	0.80	0.97	0.78	0.79	0.78	0.87	0.68		0.70		0.73		0.74	0.87
6. Vetch	WBM	0.74	0.75	0.78	0.85	0.73	0.82	0.68	0.73	0.75		0.74		0.72		0.69	0.80
	LAI	0.77	**0.80**	0.74	0.78	0.63	0.79	0.61	0.63	0.68		0.77		0.45		0.61	0.70

Figure 3. Actual versus predicted wet biomass for wheat crop. Predicted biomass was calculated using the equation $WBM = 0.1429\ e^{3.6287*NDVI920675}$. NDVI was computed using waveband centers at 920 nm and 675 nm, both with bandwidths of 15 nm. The 1:1 line had an R^2 value of 0.89.

band centered at 678 nm ($\Delta\lambda_2 = 10$) (Table 2). The visible spectrum is very sensitive to loss of chlorophyll, browning, ripening, and senescing (Idso et al., 1980); carotenoid (Tucker, 1977; Blackburn, 1998); soil background effects; and crop senescing rates and grain yield prediction (Idso et al., 1980). Changes in pigment content and chloroplast for different crop type, growth stage, and growing conditions can cause sensitivity around 568 nm and 520 nm (Nichol et al., 2000), resulting in dramatic shifts in crop-soil spectral behavior (Figures 1a through 1d). Similarly, vetch LAI is best modeled using a red-edge centered at 720 nm ($\Delta\lambda_1 = 6$) and a NIR peak centered at 910 nm ($\Delta\lambda_2 = 10$) (Table 2). Several wavebands found along the red-edge (701 nm through 740 nm) appear prominently in the best crop models (Table 2), especially for mixed growing conditions, conditions of stress, and background effects (Elvidge and Chen, 1995; Dawson and Curran, 1998; Shaw et al., 1998; Clevers, 1999). Among the other optimal bands (Table 5), band 3 ($\lambda = 550$ nm) is strongly correlated with total chlorophyll (Schepers et al., 1996), and band 1 ($\lambda = 490$ nm) with carotenoid, leaf chlorophyll, and senescing conditions (Tucker, 1977; Aoki et al., 1981; Gitelson et al., 1996). As biomass and moisture in crops increase, absorption in the moisture sensitive portion of the NIR shoulder (940 nm to 1010 nm) also increases (see Figures 1a through 1d). The mean wet biomass (kg/m²) in decreasing order of magnitude was wheat (3.28), vetch (3.22), barley (2.54), lentil (2.49), chickpea (1.41), marginal lands (0.90), and cumin (0.82). The mean spectral plots clearly indicate a significantly larger "trough" in the 940- to 1010-nm bands for vetch and lentil (Figure 1b) and for wheat and barley (Figure 1a) when compared with chickpea and cumin (Figure 1c) and marginal lands (Figure 1d). Two of the best OMBVI models (Table 3), those for cumin WBM and barley LAI, involve biomass or moisture sensitive NIR bands centered at 989 nm. Similarly, chickpea dry biomass is best estimated using a 965-nm-centered narrowband. Overall, taking the results of all TBVI and OMBVI models, a moisture sensitive NIR band centered at 975 nm ($\Delta\lambda = 15$ nm) is considered optimal (Table 5). Solar irradiant energy and the sensitivity of light

detectors are relatively higher around 960 nm than in the water absorption bands at 1450 nm and 1900 nm (Penuelas et al., 1993). It has been noted that the canopy reflectance spectrum at 960 nm detected the difference between water stressed and non-stressed canopies of rice before symptoms were visible and before NDVI could detect such a stress (Shibayama et al., 1993; Peñuelas et al., 1995). It has been noted in this study that the moisture waveband centered on 975 nm is optimal in providing crop growth information.

In all, 12 narrowbands (Table 5) and their bandwidths are determined. The importance of each of these wavebands in the study of crop characteristics is noted by providing appropriate references (Table 5).

Optimal Waveband Evaluations

The optimal bands determined in this study are compared with the optimal bands from another independent study by Thenkabail et al. (2000b), which used hyperspectral data for five summer season crops (cotton, potato, soybeans, corn, and sunflower) from 1997. In this study six rain-fed crops (wheat, barley, chickpea, lentil, cumin, and vetch) from the 1998 cropping season were used. The band centers of 10 of the 12 optimal narrowbands in this study were the same as those of Thenkabail et al. (2000b) with bandcenters within plus or minus 7 nanometers. The 12 optimal waveband centers of this study (with degree of deviations from Thenkabail et al. (2000b) provided within brackets) are $\lambda_1 = 489$ nm (+6 nm; that is, at 495 nm in Thenkabail et al. (2000)), $\lambda_2 = 518$ nm (+7 nm), $\lambda_3 = 547$ nm (+3 nm), $\lambda_4 = 575$ nm (−7 nm), $\lambda_5 = 604$ nm (none), $\lambda_6 = 661$ nm (+7 nm), $\lambda_7 = 675$ nm (+7 nm), $\lambda_8 = 704$ nm (−6 nm), $\lambda_9 = 718$ nm (+2 nm), $\lambda_{10} = 846$ nm (−1 nm), $\lambda_{11} = 904$ nm (none), and $\lambda_{12} = 975$ nm (+7 nm). These results confirm the validity of the 12 optimal hyperspectral wavebands for studying agricultural crop characteristics.

Conclusions

The study established that the optimal agricultural crop and rangeland biophysical information could be obtained using

Band number	Wavelength portion name	Band center: λ (nm)	Bandwidth: $\Delta\lambda$ (nm)	Band description or significance
1	Blue	490	30	Crop to soil reflectance ratio minima for blue and green bands. Sensitive to loss of chlorophyll, browning, ripening, senescing, and soil background effects (Thenkabail *et al.*, 1999; Thankabail *et al.*, 2000b). Very sensitive to senescing rates and is generally an excellent predictor of grain yield. Also sensitive to carotenoid pigments (Tucker, 1977; Blackburn, 1998). Blue range use is, however, questionable due to atmospheric effects and small contrast in reflectance of soil and vegetation (anonymous reviewer).
2	Green 1	520	15	Positive change in reflectance per unit change in wavelength of this visible spectrum is maximum around this "green" waveband. First order derivative plot of crop spectra will show this (e.g., Elvidge and Chen, 1995; Thenkabail *et al.*, 1999; Thenkabail *et al.*, 2000b). Nichol *et al.* (2000) found this band to be sensitive to pigment content.
3	Green 2	550	25	Green band peak (or the point maximal reflectance) in the visible spectrum. Is strongly related to total clhorophyll (Schepers *et al.*, 1996; Thenkabail, 2002).
4	Green 3	575	15	Negative change in reflectance per unit change in wavelength of the visible spectrum is maximum around this "green" wavelength. First order derivative plot of crop spectra will show this (e.g., Elvidge and Chen, 1995; Thenkabail *et al.*, 1999; Thankabail *et al.*, 2000b). Sensitive to pigment content (Nichol *et al.*, 2000).
5	Red 1	660	20	Chlorophyll absorption pre-maxima (or reflectance minima 1). Absorption in the red band (600 to 700 nm) varies significantly due to changes in factors such as biomass, LAI soil background, cultivar types, canopy structure, nitrogen, moisture, and stress in plants (Elvidge and Chen, 1995; Carter, 1997; Blackburn, 1998).
6	Red 2	675	15	Chloropyll absorption maxima anywhere in the 350- to 1050-nm range of the spectrum (or reflectance minima). Greatest crop-soil contrast is around this band center for most crops in most growing conditions (Thenkabail *et al.*, 1999; Thenkabail *et al.*, 2000b). Strong correlations with Chlorophyll a and chlorophyll b (Blackburn, 1998; Blackburn, 1999).
7	Red-edge 1	700	5	Chlorophyll absorption post-maxima (or reflectance minima 2). This is a point of sudden change in reflectance from near-maximal red absorption to beginning of the most dramatic increase in reflectance along the red-edge. Found most sensitive to plant stress and was found the most sensitive red band by Carter (1994).
8	Red-edge 2	720	15	Critical point on the red-edge around which there is maximum change in the slope of the reflectance spectra per unit change in wavelength anywhere in the 350- to 1050-nm range. First-order derivative plot of crop spectra will show this (e.g., Elvidge and Chen, 1995; Thenkabail, 2002). Sensitive to temporal variations in crop growth and condition resulting in red-edge shifts. Sensitive to vegetation stress and provides additional information about chlorophyll and nitrogen status of plants (Elvidge and Chen, 1995; Shaw *et al.*, 1998; Clevers, 1999).
9	NIR	845	120	Center of "NIR shoulder." For many crops, a broad-band or a narrow-band will provide the same result due to near uniform reflectance throughout the NIR shoulder. In such instances, other bands along the NIR shoulder will be redundant due to similar information as this waveband. Strong correlation with total clhorophyll (Schepers *et al.*, 1996).
10	NIR peak 1	905	15	Peak or maximum reflectance region of the NIR spectrum for certain types and/or growth stages of vegetation or crops. Crops such as cotton and corn or when crops are under stress or senescing there is significant change in reflectance along the "NIR shoulder" (740 to 940 nm) (Thenkabail *et al.*, 1999; Thankabail *et al.*, 2000b). Useful for computing crop moisture sensitive index (Peñuelas *et al.*, 1993).
11	NIR peak 2	920	15	Peak or maximum reflectance region of the NIR spectrum for certain other types and/or growth stages of vegetation or crops. Crops such as cotton and corn or when crops are under stress or senescing there is significant change in reflectance along the "NIR shoulder" (740 to 940 nm) (Thenkabail *et al.*, 1999; Thankabail *et al.*, 2000b).
12	NIR-Moisture sensitive	975	10	Center of the moisture sensitive "trough" portion of NIR. The "trough" portion varies from 940 to 1040 nm and typically has minimum reflectance around 975 nm (or point of maximum "dip" in the trough portion). Plant moisture sensitive band (Peñuelas *et al.*, 1995; Thenkabail *et al.*, 2000b, Thenkabail, 2002). Direct measurements of water vapor in and over vegetation canopies is feasible (Richey *et al.*, 1989).

only 12 of the 430 hyperspectral bands in the visible and near-infrared portion of the spectrum. The research was based on hyperspectral narrowband and Landsat-5 TM broadband data for six agricultural crops (barley, wheat, chickpea, lentil, vetch, and cumin) and marginal lands. Biophysical variables included leaf area index, wet and dry biomass, canopy cover, plant height, and plant nitrogen. Narrowband data were gathered using 430 discrete narrowbands, each of 1.43-nm width and in the spectral range of 395 nm to 1010 nm. Broadband data were acquired to coincide with field spectral and biophysical measurements. Data from six non-thermal bands (450 nm to 2350 nm) of Landsat-5 TM were used.

The main focus in this paper was to conduct a rigorous

evaluation of narrowband (1) two-band vegetation indices (TBVI) and (2) optimum multiple-band vegetation indices (OMBVI), and to compare them with six other categories of narrow- and broadband indices. The six other narrowband and broadband indices are red- and NIR-based normalized difference NDVI, transformed soil adjusted TSAVI, atmospheric corrected ARVI, middle-infrared-based MIVI, tassel cap greenness TCGVI, and principal-component-based PCVI. The narrowband TBVI were used to perform a rigorous search procedure involving 430 bands in order to identify the best NDVI predictors of crop biophysical variables and are illustrated using special lambda (λ_1) versus lambda (λ_2) plots of R^2 values. The piecewise linear regression models involving 430 bands are run to deter-

mine the best one-variable, two-variable, to *n*-variable narrowband OMBVI models for each crop variable.

Twelve bands provided optimal biophysical information (Table 5). The bandwidths for 11 of the 12 optimal bands are narrow (less than 30 nm). Only one band, NIR "shoulder," centered at 845 nm has broad (greater than 30-nm) bandwidth. An overwhelming proportion of crop information was concentrated in a few narrowbands (Plate 2a). The most prominent narrowbands, in order of importance, occur in the following waveband ranges: 660 to 690 nm (red-absorption maxima), 900 to 925 nm (near-infrared reflection peak), 700 and 720 nm (a portion of red-edge), and 540 to 555 nm (green reflectance maxima). These are followed by other bands that provide significant crop growth and yield information: a blue band of rapid change in slope of the spectra per unit change in wavelength centered around 490 nm; two green bands centered at 520 nm and 575 nm, providing the most rapid positive or negative change in reflectance per unit change in wavelength anywhere in the visible portion of the spectrum; the center of the NIR "shoulder" centered at 845 nm; and a biomass/moisture sensitive band centered around 975 nm. The identification of optimal bands serves two main purposes: (1) it helps select wavebands most needed for an application from hyperspectral datasets, and/or (2) it helps select wavebands for application specific sensors onboard the next generation of satellites. This study established that 418 of the 430 bands were redundant in providing agricultural crop biophysical information. These results conform with another independent study by Thenkabail *et al.* (2000b) for summer-irrigated crops in the same study area. The band centers of the 10 of the 12 optimal narrowbands in this study were the same as those of Thenkabail *et al.* (2000b), with bandcenters within plus or minus 7 nanometers. The optimal bands suggested in this paper are expected to help reduce data redundancy, data volumes, and time and resources involved in image interpretation and analysis.

Acknowledgments

References

Aoki, M., K. Yabuki, and T. Totsuka, 1981. An evaluation of chlorophyll content of leaves based on the spectral reflectivity in several plants, *Research Report of the National Institute of Environmental Studies*, Japan, 66:125–130.

Asner, G.P., C.A. Wessman, C.A., Bateson, and J.L. Privette, 2000. Impact of tissue, canopy, and landscape factors on the hyperspectral reflectance variability of arid ecosystems, *Remote Sensing of Environment*, 74(1):69–84.

Baret, F., G. Guyot, and D.J. Major, 1989. TSAVI: A vegetation index which minimizes soil brightness effects on LAI and APAR estimation, *Proceedings of the 12th Canadian Symposium on Remote Sensing, IGARRS'90*, 10–14 July, Vancouver, BC, Canada, 3:1355–1358.

Blackburn, G.A., 1998. Spectral indices for estimating photosynthetic pigment concentrations: A test using senescent tree leaves, *International Journal of Remote Sensing*, 19(4):657–675.

———, 1999. Relationships between spectral reflectance and pigment concentrations in stacks of deciduous broadleaves, *Remote Sensing of Environment*, 70(2):224–237.

Blackburn, G.A., and C.M. Steele, 1999. Relationships between spectral reflectance, pigment, and biophysical characteristics of semiarid bushland canopies, *Remote Sensing of Environment*, 70(3):278–292.

Boyd, D.S., and W.J. Ripple, 1997. Potential vegetation indices for determining global forest cover, *International Journal of Remote Sensing*, 18(6):1395–1401.

Boyd, D.S., G.M. Foody, and P.J. Curran, 1999. The relationship between the biomass of Cameroonian tropical forests and radiation reflected in middle infrared wavelengths (3.0–5.0 μm), *International Journal of Remote Sensing*, 20(5):1017–1023.

Carter, G.A., 1994. Ratios of leaf reflectance's in narrow wavebands as indicators of plant stress, *International Journal of Remote Sensing*, 15:697–703.

———, 1998. Reflectance bands and indices for remote estimation of photosynthesis and stomatal conductance in pine canopies, *Remote Sensing of Environment*, 63:61–72.

Clevers, J.G.P.W., 1999. The use of imaging spectrometry for agricultural applications, *ISPRS Journal of Photogrammetry and Remote Sensing*, 54(5–6):299–304.

Curran, P.J., J.L. Dungan, B.A. Macler, and S.E. Plummer, 1991. The effect of a red leaf pigment on the relationship between red-edge and chlorophyll concentration, *Remote Sensing of Environment*, 35:69–75.

Dawson, T.P., and P.J. Curran, 1998. A new technique for interpolating the reflectance red edge position, *International Journal of Remote Sensing*, 19(11):2133–2139.

Elmore, A.J., J.F. Mustard, S.J. Manning, and D.B. Lobell, 2000. Quantifying vegetation change in semiarid environments: Precision and accuracy of spectral mixture analysis and the normalized difference vegetation index, *Remote Sensing of Environment*, 73(1):87–102.

Elvidge, C.D., and Z. Chen, 1995. Comparison of broadband and narrow-band red and near-infrared vegetation indices, *Remote Sensing of Environment*, 54:38–48.

Elvidge, C.D., and R.J.P. Lyon, 1985. Influence of rock-soil variation on the assessment of green biomass, *Remote Sensing of Environment*, 17:265–279.

Fassnacht, K.S., S.T. Gower, M.D. MacKenzie, E.V. Nordheim, and T.M. Lillesand, 1997. Estimating the leaf area index of north central Wisconsin forests using the landsat thematic mapper, *Remote Sensing of Environment*, 61:229–245.

FieldSpec, 1997. *User's Guide, Manual Release*, Analytical Spectral Devices, Inc., Boulder, Colorado, 29 p.

Gitelson, A.A., and M.N. Merzlyak, 1996. Signature analysis of leaf reflectance spectra: Algorithm development for remote sensing of chlorophyll, *Journal of Plant Physiology*, 148(3–4):494–500.

Gong, P., R. Pu, and J.R. Miller, 1995. Coniferous forest leaf area index estimation along the Oregon transect using compact airborne spectrographic imager data, *Photogrammetric Engineering & Remote Sensing*, 61(9):1107–1117.

Huete, A.R., 1988. A soil-adjusted vegetation index (SAVI), *Remote Sensing of Environment*, 25:295–309.

Huete, A.R., R.D. Jackson, and D.F. Post, 1985. Spectral response of a plant canopy with different soil backgrounds, *Remote Sensing of Environment*, 17:37–53.

Idso, B., P.J. Pinter, Jr., R.D. Jackson, and R.J. Reginato, 1980. Estimation of grain yields by remote sensing of crop senescence rates, *Remote Sensing of Environment*, 9:87–91.

Jackson, R.D., 1983. Spectral Indices in n-Space, *Remote Sensing of Environment*, 13:409–421.

Jensen, J.R., 1996. *Introductory Digital Image Processing: A Remote Sensing Perspective*, Prentice-Hall, Inc., Upper Saddle River, New Jersey, 318 p.

Kaufman, Y.J., and D. Tanre, 1992. Atmospheric Resistant Vegetation Index, *IEEE J. Geosci. Rem. Sens.*, 30:261–270.

Lawrence, R.L., and W.J. Ripple, 1998. Comparisons among vegetation indices and bandwise regression in a highly disturbed, heterogeneous landscape: Mount St. Helens, Washington, *Remote Sensing of Environment*, 64:91–102.

Lichtenthaler, H.K., A.A. Gitelson, and M. Lang, 1996. Non-destructive determination of chlorophyll content of leaves of a green and an aurea mutant of tobacco by reflectance measurements, *Journal of Plant Physiology*, 148:483–493.

Lyon, J.G., D. Yuan, R.S. Lunetta, and C.D. Elvidge, 1998. A change detection experiment using vegetation indices, *Photogrammetric Engineering & Remote Sensing*, 64:143–150.

Mariotti, M., L. Ercoli, and A. Masoni, 1996. Spectral properties of iron-deficient corn and sunflower leaves, *Remote Sensing of Environment*, 58:282–288.

Mass, S.J., 2000. Linear mixture modeling approach for estimating cotton canopy ground cover using satellite multispectral imagery, *Remote Sensing of Environment*, 72(3):304–308.

Nichol, C.J., K.F. Huemmrich1, T.A. Black, P.J. Jarvis, C.L. Walthall, J. Grace, and F.J. Hall, 2000. Remote sensing of photosynthetic-light-use efficiency of boreal forest, *Agricultural and Forest Meteorology*, 101(2–3):131–142.

Penuelas, J., I. Filella, C. Biel, L. Serrano, and R. Save, 1993. The reflectance at the 950-970 region as an indicator of plant water status, *International Journal of Remote Sensing*, 14(10): 1887–1905.

Penuelas, J., I. Filella, P. Lloret, F. Munoz, and M. Vilajeliu, 1995. Reflectance assessment of mite effects on apple trees, *International Journal of Remote Sensing*, 16:2727–2733.

Price, J.C., 1987. Special issue on radiometric calibration of satellite data, *Remote Sensing of Environment*, 22(1):1–158.

Qi, J., A. Chehbouni, A. Huete, Y. Kerr, and S. Sorooshian, 1994. A modified soil-adjusted vegetation index (MSAVI), *Remote Sensing of Environment*, 48:119–126.

Richardson, A.J., C.L. Wiegand, D.F. Wanjura, D. Dusek, and J.L. Sreiner, 1992. Multisite analysis of spectral-biophysical data for sorphum, *Remote Sensing of Environment*, 47:71–82.

Richery, J.E., J.B. Adams, and R.L. Victoria, 1989. Synoptic-scale hydrological and biogeochemical cycles in the Amazon River Basin: A modelling and remote sensing perspective, *Remote Sensing of Biosphere Functioning*, (R.J. Hobbs and H.A. Mooney, editors), Ecological Studies 79, Springer-Verlag, New York, N.Y., pp. 249–268.

Rouse, J.W., Jr., R.H. Haas, J.A. Schell, and D.W. Deering, 1973. Monitoring vegetation systems in the Great Plains with ERTS, *Proceedings, Third ERTS Symposium*, NASA SP-351, U.S. Govt. Printing Office, Washington, D.C., 1:309–317.

SAS, 1997a. *SAS/IML User's Guide and Software Release 6.12 Edition*, SAS Institute Inc., Cary, North Carolina, 921 p.

———, 1997b. *SAS/STAT User's Guide and Software Release 6.12 Edition*, SAS Institute Inc., Cary, North Carolina, 584 p.

Schepers, J.S., T.M. Blackmer, W.W. Wilhelm, and M. Resende, 1996. Transmittance and reflectance measurements of corn leaves from plants with different nitrogen and water supply, *Journal of Plant Physiology*, 148:523–529.

Shaw, D.T., T.J. Malthus, and J.A. Kupiec, J.A. 1998. High-spectral resolution data for monitoring Scots pine (Pinus sylvestris L.) regeneration, *International Journal of Remote Sensing*, 19(13):2601–2608.

Shibayama, M., W. Takahashi, S. Morinaga, and T. Akiyama, 1993. Canopy water deficit detection in paddy rice using high resolution field Spectroradiometer, *Remote Sensing of Environment*, 45:117–126.

Thenkabail, P.S., 1999. Characterisation of the alternative to slash-and-burn benchmark research area representing the Congolese rainforests of Africa using near-real-time SPOT HRV data, *International Journal of Remote Sensing*, 20(5):839–877.

———, 2002. Optimal hyperspectral narrowbands for descriminating agricultural crops, *Remote Sensing Reviews* (in press).

Thenkabail, P.S., A.D. Ward, J.G. Lyon, and C.J. Merry, 1994. Thematic Mapper vegetation indices for determining soybean and corn crop growth parameters, *Photogrammetric Engineering & Remote Sensing*, 60(4):437–442.

Thenkabail, P.S., A.D. Ward, and J.G. Lyon, 1995. Landsat-5 Thematic Mapper models of soybean and corn crop characteristics, *International Journal of Remote Sensing*, 15:49–61.

Thenkabail, P.S., R.B. Smith, and E. De Pauw, 1999. *Hyperspectral Vegetation Indices for Determining Agricultural Crop Characteristics*, CEO Research Publication Series #1, ISBN: 0-9671303-0-1, Center for Earth Observation, Yale University, New Haven, Connecticut, 47 p.

Thenkabail, P.S., C. Nolte, and J.G. Lyon, 2000a. Remote sensing and GIS modeling for selection of a benchmark research area in the inland valley agroecosystems of West and Central Africa, *Photogrammetric Engineering & Remote Sensing*, 66(6):755–768.

Thenkabail, P.S., R.B. Smith, and E. De Pauw, 2000b. Hyperspectral vegetation indices for determining agricultural crop characteristics, *Remote Sensing of Environment*, 71:158–182.

Tucker, C.J. 1977. Spectral estimation of grass canopy variables, *Remote Sensing of Environment*, 6:11–26.

Tucker, C.J., 1980. Remote sensing of leaf water content in the near infrared, *Remote Sensing of Environment*, 10:23–32.

Vaesen, K., S. Gilliams, K. Nackaerts, and P. Coppin, 2001. Ground-measured spectral signatures as indicators of ground cover and leaf area index: the case of paddy rice, *Field Crops Research*, 69(1):13–25.

Wiegand, C.L., S.J. Mass, J.K. Aase, J.L. Hatfield, P.J. Pinter, Jr., R.D. Jackson, E.T. Kanemasu, and R.L. Lapitan, 1992. Multisite analysis of spectral-biophysical data for wheat, *Remote Sensing of Environment*, 42:1–21.